Nanoscale

RSC Publishing

COMMUNICATION

View Article Online
View Journal | View Issue

Intracellular delivery of top-down fabricated tunable nano-plasmonic resonators†

Cite this: *Nanoscale*, 2013, **5**, 10179

Received 5th June 2013
Accepted 12th August 2013

DOI: 10.1039/c3nr02910g

www.rsc.org/nanoscale

Sadao Ota,[a] Sheng Wang,[a] Jongeun Ryu,[b] Yuan Wang,[a] Yong Chen*[b] and Xiang Zhang*[a]

Engineered plasmonic structures fabricated using top-down technologies have demonstrated huge enhancements in the optical response of molecules, including Raman scattering. However, providing a sufficient number of such top-down fabricated nanostructures in solution has been a nontrivial task which has limited their potential in intracellular applications. Here we report the development of a protocol for the intracellular delivery of tunable nanoplasmonic resonators fabricated *via* scalable top-down techniques. This offers excellent possibilities towards the real-time parallel optical detection of intracellular molecular events.

The simultaneous detection of different molecules, which partake in the intracellular signaling networks within isolated biological cells, is highly demanded in many fields of biology and medicine.[1–3] For instance, mapping multiple phosphoproteins by intracellular staining is a key approach to study the complicated signaling processes in the development of cancer cells.[2–4] Fluorescence-based imaging has become the standard method of detection due to its intrinsically high signal-to-noise ratio and abundant list of available fluorophores.[5] However, the partial overlap of fluorophore emission and excitation spectra often hinders the efficacy of utilizing differently colored fluorophores and ultimately limits the number of simultaneous measurements.[6] In contrast, Raman spectroscopy allows for label-free multiple and specific molecular detection arising from molecule-specific vibrational modes.[7] However, the small spontaneous Raman scattering cross-section results in signals which are several orders of magnitude weaker than fluorescence-based methods. In order to compensate for the weaker signal, the Raman detection of biological events typically requires many emitters, ultimately limiting the spatial and/or temporal resolutions. Strong optical interactions of molecules with surface plasmons, the free electron oscillations in metals, have been utilized to demonstrate the large enhancement in Raman signals up to 10^{14} orders, potentially enabling single molecule detection.[8,9] This surface enhanced Raman scattering (SERS) effect has attracted significant scientific interests and accelerated the engineering of ideal plasmonic nanostructures for SERS.[10–13]

Chemically synthesized metallic nanoparticles have been already widely used both for *in vivo*[14] and/or *in vitro*[15] studies, extensively including SERS spectroscopy,[12] single molecule fluorescence detection,[16] and nanotoxicology.[17] These synthesized nanoparticles may be cheaply produced and easily functionalized. In contrast, the top-down fabricated nanostructures demonstrate superior tunability of resonant properties, providing high signal enhancement at desired spectral positions.[18,19] For instance, the resonant frequency of our recently developed tunable nanoplasmonic resonator (TNPR), metallic nanodiscs sandwiching a thin dielectric gap layer, is tunable by varying the physical dimensions of the discs and the gap.[20–22] The ultra-small gap between the resonators enables the extreme enhancement of the electromagnetic fields near the gap, which is important for enhancing the SERS and fluorescence signals.[20–25] The TNPRs showed among the largest single-particle enhancement of Raman scattering signals of up to 6.1×10^{10}.[20] However, these top-down nanofabrication methods such as e-beam lithography are typically limited by the slow process and high cost. Moreover, it has been challenging to release TNPRs fabricated on a solid substrate into a solution either due to their mechanical fragility, chemical contamination due to etchant, and/or the poor release and collection efficiency itself. These follow-up steps will accumulatively reduce the limited number of usable nanostructures in the final solution. Consequently, the lack of methods to prepare a great enough concentration of top-down fabricated plasmonic particles has severely limited their applications in the biological experiment as well as their quantitative argument.

[a]*Department of Mechanical Engineering, University of California, Berkeley, CA 94720, USA. E-mail: xiang@berkeley.edu; Fax: +1 510 643 2311; Tel: +1 510 642 0390*

[b]*Department of Mechanical and Aerospace Engineering, California NanoSystems Institute, University of California, Los Angeles, California 90095, USA*

† Electronic supplementary information (ESI) available: Details of fabrication methods are described. See DOI: 10.1039/c3nr02910g

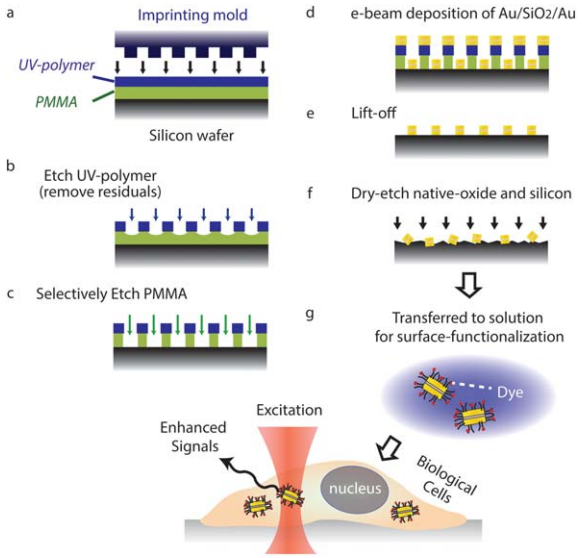

Fig. 1 The procedure for fabricating, transferring and delivering the tunable nanoplasmonic resonators (TNPRs) for the intracellular signal detection. (a) Imprinting of original nanostructured template into a large area of multi-layered polymers (UV polymer and PMMA). (b) Selective etching of the UV polymer. (c) Selective etching of PMMA. (d) e-beam deposition of gold, silicon dioxide, and gold and following lift-off (e) for fabricating massive TNPRs. (f) Dry-etching of the native silicon dioxide and following dry-etching of silicon to release the TNPRs from the silicon substrate. (g) Transfer of the released structures into a solution by sonication and following their intracellular delivery for signal detection.

In this report, we established a sequence of methods for the intracellular delivery of the massively fabricated TNPRs as drawn schematically in Fig. 1. We first fabricated a uniform array of TNPRs over a large area ($\sim 10^9$ particles per inch^2) of solid support using nano-imprinting lithography.[26,27] After dry-etching of the underpinning substrate, the TNPRs were then transferred into a solution *via* sonication and surface-functionalized with fluorescent dyes. We delivered the TNPRs into living cells and confirmed the co-localization of scattering and fluorescence signals from the TNPRs. In addition, the fabricated structures are designed to exhibit resonances in the near-IR range, matching the biologically transparent optical window (800–1200 nm),[28] ideal for Raman intracellular signal detection.

The fabrication of the TNPRs started with nanoimprinting lithography since it allows one to simultaneously fabricate a massive number (1.6×10^9 per sample) of uniform nanostructures. Using the nanoimprinted mold and standard e-beam evaporation (Fig. 1a–e), we obtained a uniform TNPR array with a TNPR diameter of 150 nm and periodicity of 500 nm on the silicon surface (Fig. 1e as well as Fig. 2a for the SEM image of the fabricated TNPR array pattern). The fabricated TNPRs are gold nanodiscs of 20 nm thickness sandwiching a thin silicon dioxide layer of 5 nm thickness. After removing the residual polymer *via* oxygen plasma cleaning, the top-down fabricated nanostructures were released and transferred into water without chemically contaminating their surfaces using the dry-etching procedure shown in Fig. 1f and 2. In this process, we first removed the native oxide using HF-vapor with a solution temperature maintained at 30 degree Celsius while the sample holder was kept at 40 degree Celsius for one minute (Fig. 2b). Excessive etching due to a lower temperature or increased time caused the gold structures to embed deeply into the silicon substrate, possibly due to metal-enhanced chemical etching (Fig. 2c).[29] Since the nanostructures are still intact with the bottom substrate, a final dry-etching of 200 nm of the underlying silicon by xenon-difluoride gas was required for particles' complete release (Xetch, XACTIX, PA in USA). The released TNPRs were transferred into a solution by covering the substrate with a small droplet of de-ionized (DI) water followed by sonication for five minutes. Fig. 2d and its inset show the SEM images of the random distribution of the released TNPRs. Fig. 2e shows that most of the TNPRs were efficiently transferred into a solution after sonication. The solution was separated from the substrate and stored in a small glass bottle. By drying the final solution on a solid substrate, the concentrated particles were collected as shown in the SEM image (the inset of Fig. 2e). A zoom-in SEM image of the released particles clearly shows that the oxide gap remains between the metallic nanodiscs after the final release (Fig. 2f).

The TNPRs with bare gold surfaces in the DI water are functionalized with organic emitter molecules. They were incubated with 1 μg ml^{-1} Texas Red conjugated goat anti-mouse IgG (Santa Cruz biotechnology) for 2 h. The sample was rinsed with 1× PBS, pH 7.4, three times through centrifuging down the TNPRs and removing the supernatant liquid. The successful

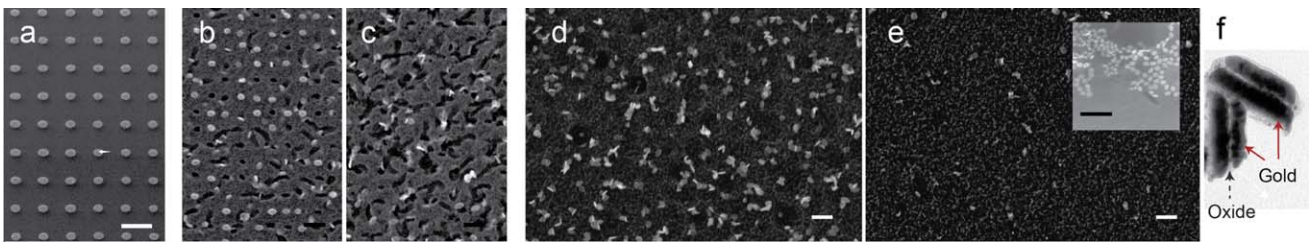

Fig. 2 SEM images of the TNPRs in the progress of their transfer into an aqueous solution. (a) TNPRs fabricated by nanoimprinting lithography (Fig. 1e). For (a–e), scales bars are 500 nm. (b and c) After short- and long time dry-etching of substrate layers (Si and its native oxide) underpinning the TNPRs using HF vapor, showing the metal-enhanced etch due to the catalytic effect of the gold in TNPRs. The excessive etch needs to be considered as it causes the irreversible immobilization of the nanostructures in the substrate. (d) A SEM image of the released TNPRs after dry etching of the silicon substrate by XeF_2 gas and the inset shows its zoomed-in image. (e) A SEM image of the same sample after sonication under an aqueous droplet for 10 minutes, showing the absence of TNPRs due to their transfer into the solution. After drying the final solution on another substrate, the aggregated TNPRs were found to confirm the successful transfer (inset). (f) shows the TEM image of the released TNPRs, showing a thin dielectric layer between the gold discs.

surface coating with fluorophores prevented aggregation of the particles, allowing us to keep the solution in a glass bottle at least for a week. The intracellular delivery of the surface-labeled TNPRs was performed simply by incubating plated HEK 293 cells with TNPRs in cell culture medium (DMEM with 5% fetal bovine serum) overnight. After rinsing with 1× PBS, a live–dead cell assay was performed. Briefly, the cells were covered by a live–dead assay reagent (2 μM of calcein AM and 4 μM EthD-1 in D-PBS solution), incubated for 30 min, and then washed with a clean D-PBS solution for imaging. Fig. 3a shows the dark-field image of the cultured cells, showing that the TNPRs had internalized in the cellular bodies as bright scattering spots. Fig. 3b shows a fluorescence image of the same field of view taken with a 645/70 nm emission filter, showing fluorescence emission from the labeling dyes (Texas-Red) on the TNPRs. Fig. 3c also shows a fluorescence image of the same view, but taken with a 535/50 nm filter, showing that cells were alive. The positions of the red dyes in Fig. 3b corresponded to those of TNPRs in Fig. 3a, as shown in the overlap image (Fig. 3d). This result confirms the successful intracellular delivery of the surface-functionalized plasmonic nanostructures by this protocol.

The successful delivery of the TNPRs is a significant step towards the detection of SERS signals within the living cells. In this work, the fluorescence labeling conveniently proved the successful surface functionalization and intracellular delivery *via* co-localization imaging. In order to utilize the TNPRs for intracellular SERS detection, the resonance frequency needs to match the biologically transparent optical window (800 nm to 1200 nm).[28] This matching not only reduces the background noise, but also enhances the SERS signals by exciting the adsorbed molecules at its absorption band, allowing for signal collection even in deep tissues.[30] Fig. 4 shows the comparison between the measured transmission spectrum of the as-fabricated TNPRs in air and that of the released TNPRs in water. The measurement was performed by applying the non-polarized light to the massive number of TNPRs, where slight polarization dependence of its shape is averaged out as expected in the real intracellular applications. The red-shift of the resonance peak from 750 nm to 810 nm is due to the higher refractive index of water as opposed to air. We also simulated the optical response of the TNPRs on a glass substrate either in water or in air using COMSOL Multiphysics. A plane wave was applied as a background and scattering components of the electromagnetic power flows were integrated for characterizing the resonance spectrum. The optical response of the gold was described by a dielectric function with a Drude–Lorentz model,

$$\varepsilon(\omega) = 1 - \frac{{\omega_p}^2}{\omega^2 + i\frac{\omega}{\tau}} \quad (1)$$

where ω_p is the plasma frequency of 1.2×10^{16} s^{-1}, τ is the collision time of 7×10^{-15} s, and ω is the angular frequency of light.[31] The successful agreement between the experimental measurement and numerical calculation proved that our engineered nanostructures fall in the near IR range as designed.

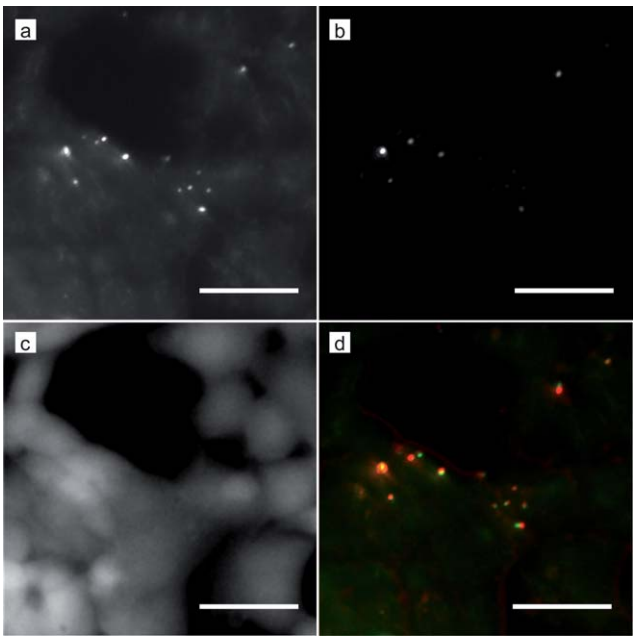

Fig. 3 (a) Dark-field image of the biological cells after co-culturing with the fluorescently labeled TNPRs. The bright scattering spots show the internalized TNPRs. (b) Fluorescence image of the same sampled cells, showing fluorescence signals emitted from the labeling dyes (Texas-Red) on TNPRs within the cells. (c) Meanwhile, the live–dead cell assay confirmed that the cells were alive. (d) Overlapped dark-field ((a) with pseudo-green) and fluorescence images ((b) with red for labeling dyes) show their co-localization, confirming that intercellular delivery of the labeling dyes attached on the TNPRs. Scale bars: 20 μm.

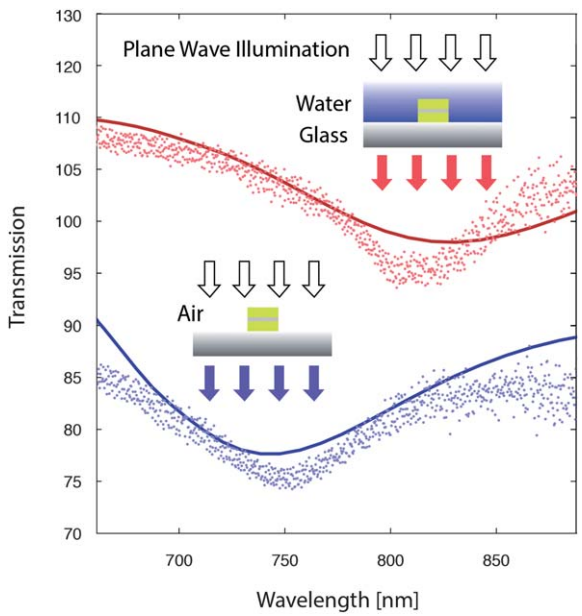

Fig. 4 Absorption spectrum of the TNPRs in air (blue) and that in water (red) on a glass cover slip. Dots are the experimental measurements while solid curves are numerical simulations. In the experiment, a normal tungsten lamp was used to collect the transmission light and a spectrometer (Horiba) was used for the measurement. The addition of water, whose refractive index is higher than that of air, resulted in the red shift of their absorption peak. The curve for the TNPRs in water is displayed with an offset.

Conclusions

In summary, we have demonstrated the intracellular delivery of the top-down fabricated nanoplasmonic resonators for the first time. The delivery was enabled by developing a protocol for the efficient preparation of a large number of nanostructures in a solution: scalable fabrication of the TNPRs by nanoimprinting, high-yield release by substrate-etching, direct transfer into a solution by sonication, and the effective surface functionalization. The top-down method also enables the fine control of physical dimensions of the TNPRs which determine the optical resonance properties, such as Raman scattering. We believe this technology will serve as a powerful platform for the simultaneous detection of different signaling molecules inside living cells.

Acknowledgements

This work is financially supported by the National Science Foundation Nano-scale Science and Engineering Center (NSF-NSEC) for Scalable and Integrated NanoManufacturing (SINAM) (Grant No. CMMI-0751621), and the National Institutes of Health through the NIH Roadmap for Medical Research (PN2 EY018228).

Notes and references

1 S. F. Kingsmore, *Nat. Rev. Drug Discovery*, 2006, **5**, 310–321.
2 M. P. Bruchez, *Curr. Opin. Chem. Biol.*, 2005, **9**, 533–537.
3 P. Lang, K. Yeow, A. Nichols and A. Scheer, *Nat. Rev. Drug Discovery*, 2006, **5**, 343–356.
4 P. K. Chattopadhyay, D. A. Price, T. F. Harper, M. R. Betts, J. Yu, E. Gostick, S. P. Perfetto, P. Goepfert, R. A. Koup, S. C. De Rosa, M. P. Bruchez and M. Roederer, *Nat. Med.*, 2006, **12**, 972–977.
5 S. P. Perfetto, P. K. Chattopadhyay and M. Roederer, *Nat. Rev. Immunol.*, 2004, **4**, 648–655.
6 M. Roederer, *Cytometry*, 2001, **45**, 194–205.
7 K. Kneipp, H. Kneipp, I. Itzkan, R. R. Dasari and M. S. Feld, *Chem. Rev.*, 1999, **99**, 2957–2976.
8 S. Nie and S. R. Emory, *Science*, 1997, **275**, 1102–1106.
9 K. Kneipp, Y. Wang, H. Kneipp, L. T. Perelman, I. Itzkan, R. R. Dasari and M. S. Feld, *Phys. Rev. Lett.*, 1997, **78**, 1667–1670.
10 G. A. Baker and D. S. Moore, *Anal. Bioanal. Chem.*, 2005, **382**, 1751–1770.
11 J. J. Baumberg, T. A. Kelf, Y. Sugawara, S. Cintra, M. E. Abdelsalam, P. N. Bartlett and A. E. Russell, *Nano Lett.*, 2005, **5**, 2262–2267.
12 J. B. Jackson and N. J. Halas, *Proc. Natl. Acad. Sci. U. S. A.*, 2004, **101**, 17930–17935.
13 P. L. Stiles, J. A. Dieringer, N. C. Shah and R. P. Van Duyne, *Annu. Rev. Anal. Chem.*, 2008, **1**, 601–626.
14 C. Höppener and L. Novotny, *Nano Lett.*, 2008, **8**, 642–646.
15 F. Tam, G. P. Goodrich, B. R. Johnson and N. J. Halas, *Nano Lett.*, 2007, **7**, 496–501.
16 P. Anger, P. Bharadwaj and L. Novotny, *Phys. Rev. Lett.*, 2006, **96**, 113002.
17 G. Oberdörster, E. Oberdörster and J. Oberdörster, *Environ. Health Perspect.*, 2005, **113**, 823–839.
18 S. Lal, S. Link and N. J. Halas, *Nat. Photonics*, 2007, **1**, 641–648.
19 F. Hao, Y. Sonnefraud, P. V. Dorpe, S. A. Maier, N. J. Halas and P. Nordlander, *Nano Lett.*, 2008, **8**, 3983–3988.
20 K.-H. Su, S. Durant, J. M. Steele, Y. Xiong, C. Sun and X. Zhang, *J. Phys. Chem. B*, 2006, **110**, 3964–3968.
21 K. H. Su, Q. H. Wei and X. Zhang, *Appl. Phys. Lett.*, 2006, **88**, 063118.
22 K. H. Su, Q. H. Wei, X. Zhang, J. J. Mock, D. R. Smith and S. Schultz, *Nano Lett.*, 2003, **3**, 1087–1090.
23 M. Moskovits, *J. Raman Spectrosc.*, 2005, **36**, 485–496.
24 S. Wang, S. Ota, B. Guo, J. Ryu, C. Rhodes, Y. Xiong, S. Kalim, L. Zeng, Y. Chen, M. A. Teitell and X. Zhang, *Nano Lett.*, 2011, **11**, 3431–3434.
25 C. Sun, K.-H. Su, J. Valentine, Y. T. Rosa-Bauza, J. A. Ellman, O. Elboudwarej, B. Mukherjee, C. S. Craik, M. A. Shuman, F. F. Chen and X. Zhang, *ACS Nano*, 2010, **4**, 978–984.
26 S. Y. Chou, P. R. Krauss and P. J. Renstrom, *Science*, 1996, **272**, 85–87.
27 B. D. Gates, Q. Xu, M. Stewart, D. Ryan, C. G. Willson and G. M. Whitesides, *Chem. Rev.*, 2005, **105**, 1171–1196.
28 P. Hildebrandt and M. Stockburger, *J. Phys. Chem.*, 1984, **88**, 5935–5944.
29 X. Li, *Curr. Opin. Solid State Mater. Sci.*, 2012, **16**, 71–81.
30 B. J. Tromberg, N. Shah, R. Lanning, A. Cerussi, J. Espinoza, T. Pham, L. Svaasand and J. Butler, *Neoplasia*, 2000, **2**, 26–40.
31 M. Kreiter, S. Mittler, W. Knoll and J. Sambles, *Phys. Rev. B: Condens. Matter Mater. Phys.*, 2002, **65**, 125415.

